The temperature increase in carbon materials during magic-angle spinning solid-state nuculear magnetic resonance measurements

Hata, Koichiro
Interdisciplinary Graduate School of Engineering Sciences, Kyushu University

Ideta, Keiko
Institute for Materials Chemistry and Engineering, Kyushu University

Toda, Shigemi
Tokai Carbon Co., Ltd.

Nakabayashi, Koji
Interdisciplinary Graduate School of Engineering Sciences, Kyushu University

他

https://hdl.handle.net/2324/7331616

出版情報：Carbon Reports. 2 (3), pp.179-184, 2023-09-01. 炭素材料学会
バージョン：

Research Paper
Carbon Reports
Vol. 2 No. 3 2023 179-184

The temperature increase in carbon materials during magic-angle spinning solid-state nuculear magnetic resonance measurements

Koichiro Hata[a)], Keiko Ideta[b)], Shigemi Toda[c)], Koji Nakabayashi[a),b)], Isao Mochida[b)], Seong-Ho Yoon[a),b)] and Jin Miyawaki[a),b),*]

a) Interdisciplinary Graduate School of Engineering Sciences, Kyushu University: 6–1 Kasuga-koen, Kasuga, Fukuoka 816–8580, Japan
b) Institute for Materials Chemistry and Engineering, Kyushu University: 6–1 Kasuga-koen, Kasuga, Fukuoka 816–8580, Japan
c) Tokai Carbon Co., Ltd.: 1–2–3 Kita-aoyama, Minato-ku, Tokyo 107–8636, Japan

The structure of carbon materials and their precursors can be studied by magic-angle spinning solid-state nuclear magnetic resonance (MAS-SS-NMR). The state and structure of adsorbed and/or intercalated molecules and ions on/in the carbon materials can also be determined using this method. Eddy currents induced by the magnetic field during measurements cause a temperature increase in conducting carbon materials. The effects of various physical and chemical characteristics of the carbon materials on this temperature increase were investigated. The oxygen content was found to be the dominant factor determing the temperature increase, with a higher oxygen content giving a smaller temperature increase. This correlation enables a rough estimate of the temperature increase in carbon materials prior to performing MAS-SS-NMR measurements.

KEYWORDS: Temperature increase, Conducting carbon materials, Magic-angle spinning solid-state nuclear magnetic resonance, Eddy current, Oxygen content

1. Introduction

Various carbon materials, including graphite, hard carbon, activated carbon (AC), and carbon black (CB), are used as electrode materials or conductive auxiliary agents in batteries and electric double layer capacitors [1–4]. Solid-state nuclear magnetic resonance (SS-NMR) is used to investigate the storage state, storage mechanism, and stability of ions [5–7]. This is because SS-NMR can provide element-selective and local-environment-sensitive information on target ions, even if they are intercalated in or adsorbed on carbon materials [8–10]. The underlying principle of SS-NMR is similar to that of common liquid-state NMR, but the mobility of solid samples is much lower than that of liquid samples. Because the NMR peak line width is related to mobility, solid samples often show broader peaks than liquid samples. Therefore, high-speed magic-angle spinning (MAS) is often used to decrease the anisotropy of solid samples to obtain sharp peaks. Recent developments in MAS probes enable ultrahigh MAS speeds on the scale of tens of kHz [11, 12].

It is well known that the motion of conductive materials in a magnetic field and the application of magnetic-field gradients to conductive materials induce eddy currents. These phenomena occur in the magnetic fields during NMR and magnetic resonance imaging (MRI) measurements [13–15]. The eddy currents result in broadened resonances and distorted lineshapes, preventing accurate NMR measurements and MRI diagnostics. In addition, the electrical resistance of the specimen causes the transformation of the generated eddy current into heat [16]. The larger the eddy current generated, the higher the temperature increase. For some nuclear species, the change in temperature causes a substantial change in the NMR chemical shift and thus inaccurate analysis results [17–20]. Furthermore, physical and chemical transformations of carbon materials, additives, and/or electrolytes may be induced by an increase in temperature. If a specimen melts because of the temperature increase, it may leak from the NMR sample tube owing to the centrifugal force induced by the high-speed MAS. This would result in the contamination of the NMR apparatus. If the electrolyte decomposes with the gas generation, there is a risk that the cap of the sample tube will burst off and seriously damage the NMR apparatus. To avoid such occurrences, it is important to

* Corresponding Author, E-mail: miyawaki@cm.kyushu-u.ac.jp
https://doi.org/10.7209/carbon.020304
(Received May 5, 2023, Accepted July 3, 2023)
(J-STAGE Advance published July 11, 2023)

estimate the magnitude of temperature increase in the sample prior to performing MAS-SS-NMR measurements.

The size of the generated eddy current is thought to be affected by various factors such as the strength of the NMR magnetic field, the MAS speed, the electrical conductivity of the sample, and the packing density of the sample. Among these factors, the strength of the NMR magnetic field and the MAS speed depend on the apparatus and measurement conditions. At the same time, different carbon materials have different electrical conductivities. Accurate measurement of the intrinsic intra-particle electrical conductivity of powdered carbon materials is difficult because the measured apparent electrical conductivity is affected by inter-particle contact resistance and packing density. Furthermore, intra-particle electrical conductivity is considered a function of the physicochemical properties of the carbon material. These properties include the level of graphitic structure development, particle size, and chemical composition.

In this study, the critical properties determining the temperature increase during MAS-SS-NMR measurements of carbon materials were investigated. Various powdered carbon materials with different degrees of graphitization, contents of surface functional groups, porosity, and particle size were considered. In ^{207}Pb-NMR spectra, the chemical shifts are known to correlate well with temperature changes [17–19, 21, 22]; thus, *in situ* temperature measurements of carbon materials were performed during MAS-SS-NMR with $Pb(NO_3)_2$ mixed into the carbon samples as a temperature indicator. The oxygen content of the carbon material was found to be the determining factor for the magnitude of temperature increase caused by the generated eddy currents during MAS-SS-NMR. For example, Ketjen black, which contains a relatively low number of oxygen-containing surface functional groups, induced a maximum local temperature increase of about 75 °C at the MAS speed of 10 kHz in a 400-MHz NMR apparatus. On the other hand, oxygenated carbon materials showed a temperature increase of less than 20 °C under the same experimental conditions. Furthermore, a correlation between oxygen content and temperature increase was obtained regardless of the differences in the parent carbon material, enabling the prediction of temperature increase during MAS-SS-NMR measurements.

2. Experimental

Three types of CB and one type of AC were used as parent samples in this study. CBs were supplied by Tokai Carbon Co., Ltd., Japan (furnace black; FB), Denka Co., Ltd., Japan (acetylene black; AB), and Lion Specialty Chemicals Co., Ltd., Japan (Ketjen black ECP; KB). AC was provided by Kansai Coke and Chemicals Co., Ltd., Japan (MSC30, MAX). Oxidation treatment was performed by exposing about 100 g of each CB or AC specimen to an O_3/O_2 gas mixture (O_3; 12 g/h, 39 g/m^3) at room temperature for 7 h. The O_3/O_2 gas mixture was generated using a commercial ozone generator (CO-101, Ishimori Co., Ltd., Japan). The oxidized FB, AB, KB, and MAX are further referred to as Ox-FB, Ox-AB, Ox-KB, and Ox-MAX, respectively. Samples with a lower oxygen content were prepared through the heat treatment of as-received CB and AC samples in a reducing atmosphere (Ar/H_2=8/2 (v/v)) at 600 °C for 24 h (further referred to as H-FB, H-AB, H-KB, and H-MAX, respectively). Non-conductive SiO_2 powder (325 mesh, 99.6% purity; Sigma-Aldrich Co., USA) was used as a reference sample without any purification.

Elemental compositions of the samples were determined using a CHN analyzer (MT-5, Yanako, Japan). Oxygen content ($O_{diff.}$) was determined by subtracting the sum of C, H, and N contents from 100%. Raman spectra were acquired at room temperature (NRS-3200, JASCO Co., Japan). *R* values (I_D/I_G values) were calculated from the ratio of intensities at 1350 and 1580 cm^{-1}. Average interlayer spacings, d_{002}, were obtained according to the Gakushin method [23] using an X-ray diffraction (XRD) apparatus (RINT-Ultima III, Rigaku, Japan). Specific surface areas (SSA) of CBs and ACs were calculated *via* the Brunauer–Emmett–Teller method [24] (analyzed relative pressure range: P/P_0=0.05–0.35) and the α_S method [25], respectively, from N_2 adsorption isotherms measured at 77 K using a volumetric adsorption apparatus (BELSORP-max-S, BEL Japan Inc., Japan). The samples were heated at 150 °C in vacuum for 2 h prior to the adsorption measurements. ^{207}Pb-NMR spectra were used to estimate the temperature of samples during MAS-SS-NMR measurements. Each sample was mixed with 10 wt.% $Pb(NO_3)_2$ powder (>99.9% purity, Wako Pure Chemical Industries, Ltd., Japan). A 400-MHz, solid-state NMR (JNM-ECX-400, JEOL Ltd., Tokyo, Japan) was used to acquire ^{207}Pb-NMR spectra at room temperature. Prior to the NMR measurements, samples were preheated at 100 °C under N_2 gas flow for 2 h and then packed in a 3.2 mm ZrO_2 NMR sample tube using a sampling stick under N_2 atmosphere. The NMR measurements were conducted using a cross polarization/magic-angle spinning probe at 3.5 μs with a 90° pulse angle, a relaxation delay of 10 s, and different MAS speeds. Typically, 1024–8192 scans were performed to obtain spectra with reliable signal-to-noise ratios. The measurement times in this study were at levels typical for SS-NMR measurements [9, 26].

3. Results and Discussion

The oxygen contents, $O_{diff.}$, of the CB and AC samples are listed in **Table 1**. The $O_{diff.}$ values increased after the oxidation treatment and decreased after the reduction treatment regardless of the parent carbon material. It has been reported that ozonation at room temperature preferentially generates acidic surface functional groups, especially carboxylic groups [27, 28], whereas ozone treatment at elevated temperatures decreases the content of carboxylic groups [29]. SSA, I_D/I_G, and d_{002} values for each sample are also presented in **Table 1**.

Although CBs show a broad but clear d_{002} peak in their XRD pat-

Table 1 Physical and chemical properties of CBs and ACs.

Sample	SSA [m^2 g^{-1}]	I_D/I_G [−]	d_{002} [Å]	Elemental composition [mass%]			
				C	H	N	$O_{diff.}$ [b]
Ox-FB	88	1.02	3.700	93.47	0.53	0.21	5.79
FB	76	1.03	3.702	95.33	0.61	0.25	3.81
H-FB	82	1.02	3.668	97.96	0.42	0.33	1.29
Ox-AB	342	1.37	3.515	74.69	0.33	0.03	24.95
AB	321	1.84	3.826	98.21	0.32	0.13	1.34
H-AB	333	1.63	3.800	98.94	0.07	0.12	0.87
Ox-KB	333	1.13	3.468	72.30	0.39	0.05	27.26
KB	816	1.18	3.625	98.45	0.23	0.05	1.27
H-KB	813	1.33	3.701	98.68	0.21	0.03	1.08
Ox-MAX	2618	1.01	–[a]	91.05	0.36	0.15	8.44
MAX	3045	1.02	–[a]	95.13	0.14	0.25	4.48
H-MAX	3029	1.04	–[a]	97.91	0.22	0.12	1.75

[a]Not available because of unclear d_{002} peak for ACs. [b]$O_{diff.}$ [mass%]=100−(C+H+N).

terns (Supporting Information, **Fig. S1**), this peak is not observed for ACs (MAX series). The oxidation treatment considerably reduced the d_{002} values of the AB and KB series, suggesting an improvement in graphitic stacking alignment. It has been previously reported that the oxidation of ABs with small particle sizes improves crystallinity by releasing the strain of the curved graphitic structure [30]. Regarding the specific surface areas, no remarkable changes are observed after the oxidation or reduction treatments, except for a significant decrease in the SSA of KB after oxidation. A thin shell of stacked graphene sheets of KB was considered less robust than those of other CBs [31].

Fig. 1 shows ^{207}Pb-NMR spectra of $Pb(NO_3)_2$ without any carbon samples at different MAS speeds. Hereafter, the peak position at a MAS speed of 2 kHz is considered 0 ppm. In the ^{207}Pb-NMR spectra, the higher the MAS speed, the more pronounced the deshielded shift (high-ppm shift) in the peak position. As mentioned above, the chemical shifts of peaks in ^{207}Pb-NMR spectra are known to be highly correlated with temperature [17–19, 21, 22]. The deshielded shift indicates an increase in temperature, and peak broadening indicates the widening of the temperature distribution. Using the previously reported correlation ($\delta=T\times0.753$ [ppm/°C]) [17], the observed chemical shift of the peak in the ^{207}Pb-NMR spectra was converted to temperature increase, $\Delta T_{obs.}$, as shown in **Fig. 1**. The value of $\Delta T_{obs.}$ increases at an accelerated pace with increasing MAS speed. In the case of $Pb(NO_3)_2$ alone, the observed shifts in the signal were primarily attributed to the unavoidable temperature increase caused by air friction of the NMR sample tube rotating at a high speed, ΔT_{AF}. Indeed, similar degrees of deshielded shift are observed in the experiments conducted with $Pb(NO_3)_2$ without any carbon samples using an NMR apparatus with a higher magnetic field, as shown in **Fig. S2** (Supporting Information). A higher temperature increase, *i.e.*, a greater deshielded shift, should be observed in higher magnetic fields if it is caused by eddy currents. Furthermore, the ^{207}Pb-NMR spectra of non-conductive SiO_2 powder mixed with 10 wt.% $Pb(NO_3)_2$ agreed

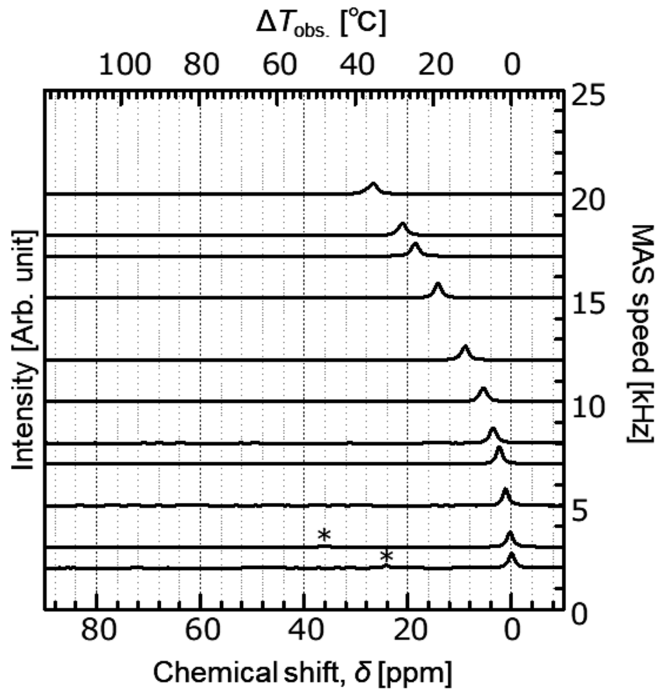

Fig. 1 ^{207}Pb-NMR spectra of $Pb(NO_3)_2$ at different MAS speeds using a 400-MHz NMR apparatus. The peaks marked by * denote the spinning sidebands.

with those of $Pb(NO_3)_2$ alone (Supporting Information, **Fig. S2**). This also indicated that the eddy current-induced temperature increase in $Pb(NO_3)_2$ alone or in non-conductive materials was negligible, that is $\Delta T_{obs.}\approx\Delta T_{AF}$.

The ^{207}Pb-NMR spectra of carbon materials mixed with 10 wt.% $Pb(NO_3)_2$ obtained at different MAS speeds are shown in **Fig. 2**. Compared with neat $Pb(NO_3)_2$, larger deshielded shifts are observed for all the CB and AC samples at the same MAS speeds. This indicates that in addition to the temperature increase caused by air friction of the high-speed rotating NMR sample tube, an extra temperature increase was induced in carbon materials, probably due to the generated eddy currents. Furthermore, higher deshielded shifts

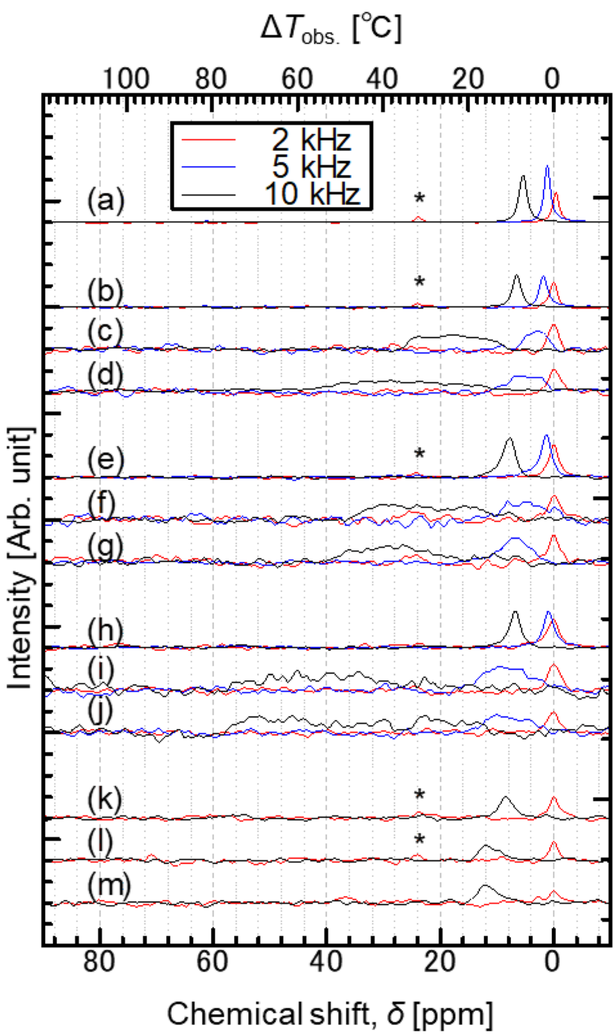

Fig. 2 [207]Pb-NMR spectra of CBs and ACs mixed with 10 wt.% $Pb(NO_3)_2$ at MAS speeds of 2, 5, and 10 kHz using a 400-MHz NMR apparatus: (a) $Pb(NO_3)_2$ alone, (b) Ox-FB, (c) FB, (d) H-FB, (e) Ox-AB, (f) AB, (g) H-AB, (h) Ox-KB, (i) KB, (j) H-KB, (k) Ox-MAX, (l) MAX, and (m) H-MAX. The peaks marked by * denote the spinning sidebands.

resulted in a greater broadening of the spectral peak. This indicated wider temperature distributions, which were not so pronounced for $Pb(NO_3)_2$ alone. The degree of the deshielded shift and peak broadening by the high-speed MAS varied for each sample. These parameters depend on the type of parent carbon material and the treatment that the sample underwent. For example, the temperature increase observed in oxidized CBs and Ox-MAX is approximately constant (9–12 °C). In this case, eddy currents contributed at most 4 °C to the temperature increase. Conversely, for KB and H-KB, maximum local temperature increases reached about 75 °C, which may cause degradation and decomposition of electrolytes if these carbon materials are used as conductive auxiliary agents in battery cells.

The results shown in **Fig. 2** indicate that the eddy current–generated temperature increases vary in different carbon materials. The relationships between the temperature increase and the I_D/I_G, d_{002}, and $O_{diff.}$ values, which were considered to affect the intrinsic electrical conductivity of carbon materials, were examined to clarify which of these properties most strongly influences the temperature increase. **Fig. 3** shows the correlation between each parameter and the average temperature increase due to generated eddy currents at a MAS speed of 10 kHz, ΔT_{EC}, which was calculated using the following equation

$$\Delta T_{EC} = \Delta T_{obs.} - \Delta T_{AF},$$

where $\Delta T_{obs.}$ is the observed temperature increase above room temperature for the carbon sample mixed with 10 wt.% $Pb(NO_3)_2$, and ΔT_{AF} is that for $Pb(NO_3)_2$ alone. Here, the values of ΔT_{AF} and $\Delta T_{obs.}$ were averaged temperature increases estimated from the smallest and largest chemical shifts of each spectrum because of the difficulties in determining the peak top position, especially for broad NMR peaks at the MAS speed of 10 kHz.

The use of results for $Pb(NO_3)_2$ alone allows to exclude the contribution of air friction. Although no correlations were detected between

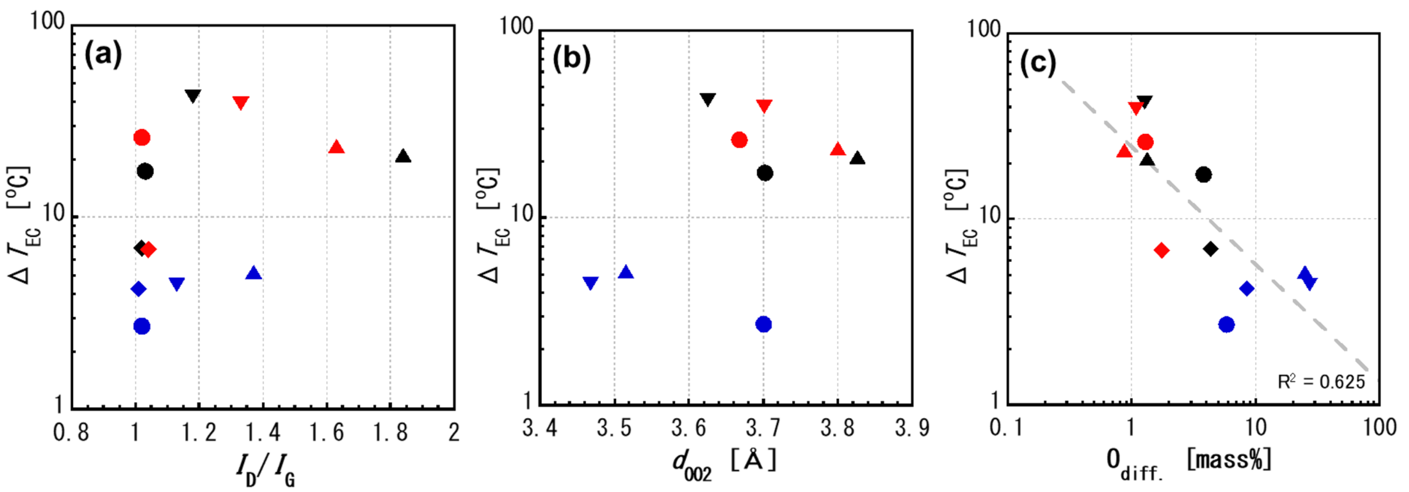

Fig. 3 Correlation between eddy current-induced temperature increase, ΔT_{EC}, at a MAS speed of 10 kHz in a 400-MHz NMR apparatus and (a) I_D/I_G, (b) d_{002}, and (c) $O_{diff.}$ values of CBs and ACs. (circles) FBs, (triangles) ABs, (inverted triangles) KBs, and (diamonds) ACs. The black-, blue-, and red-colored symbols denote pristine, oxidized, and reduced samples, respectively.

I_D/I_G or d_{002} and ΔT_{EC} (**Fig. 3**(a) or (b)), $O_{diff.}$ was roughly correlated with ΔT_{EC}, as shown in **Fig. 3**(c). Higher $O_{diff.}$ values yielded lower ΔT_{EC} values. The suppression of temperature increase with an increase in $O_{diff.}$ was most likely due to a decrease in the electron density of the hexagonal carbon layers. This is caused by electron-withdrawing oxygen-containing surface functionalities such as carboxylic groups [32]. It should be noted that the CB and AC samples exhibit similar $O_{diff.}$–ΔT_{EC} correlation curves, regardless of differences in porosity (CBs are non-porous or moderately porous, but ACs are highly porous) and particle size (tens of nanometers for CBs, but tens of micrometers for ACs), as presented in **Table 1** and **Fig. S3** (Supporting Information), respectively. Oxygen-containing surface functional groups should be introduced not only onto the external surface of carbon materials but also onto the internal surface of any pores such as those in ACs. Therefore, the unitary correlation between $O_{diff.}$ and ΔT_{EC} observed for all investigated carbon materials suggests that the magnitude of the generated eddy current is independent of the location of introduced oxygen-containing surface functionalities. It also suggests that the temperature increase in carbon materials can be roughly estimated using the correlation shown in **Fig. 3**(c) prior to the MAS-SS-NMR measurements.

4. Conclusions

Conductive carbon materials generate eddy currents that induce temperature increase in addition to that caused by air friction during MAS-SS-NMR measurements. The magnitude of this phenomenon depends on the parent carbon material and the chemical treatment it underwent. Among the properties considered, the oxygen content of carbon materials determined the electron density in hexagonal carbon layers and the magnitude of generated eddy currents. Thus, oxygen content governed the degree of eddy current–induced temperature increase in carbon materials during MAS-SS-NMR measurements.

References

[1] Y. Kado, Y. Soneda, H. Hatori, M. Kodama, Advanced carbon electrode for electrochemical capacitors, J. Solid State Electrochem. 23 (2019) 1061–1081.

[2] L. Xie, C. Tang, Z. Bi, M. Song, Y. Fan, C. Yan, X. Li, F. Su, Q. Zhang, C. Chen, Hard carbon anodes for next-generation Li-ion materials: Review and perspective, Adv. Energy Mater. 11 (2021) 2101650.

[3] Z. Wu, K. Sun, Z. Wang, A review of the application of carbon materials for lithium metal batteries, Batteries 8 (2022) 246.

[4] K. Yanamandra, D. Pinisetty, N. Gupta, Impact of carbon additives on lead-acid battery electrodes: A review, Renew. Sustain. Energy Rev. 173 (2023) 113078.

[5] K. Gotoh, ^{23}Na solid-state NMR analyses for Na-ion batteries and materials, Batter. Supercaps 4 (2021) 1267–1278.

[6] M. Liu, C. Wang, C. Zhao, E. van der Maas, K. Lin, V.A. Arszelewska, B. Li, S. Ganapathy, M. Wagemaker, Quantification of the Li-ion diffusion over an interface coating in all-solid-state batteries via NMR measurements, Nat. Commun. 12 (2021) 5943.

[7] X. Liu, Z. Liang, Y. Xiang, M. Lin, Q. Li, Z. Liu, G. Zhong, R. Fu, Y. Yang, Solid-state NMR and MRI spectroscopy for Li/Na Batteries: Materials, Interface, and in situ characterization, Adv. Mater. 33 (2021) 2005878.

[8] H. Fujimoto, A. Mabuchi, K. Tokumitsu, N. Chinnasamy, T. Kasuh, ^{7}Li nuclear magnetic resonance studies of hard carbon and graphite/hard carbon hybrid anode for Li ion battery, J. Power Sources 196 (2011) 1365–1370.

[9] L.A. Huff, J.L. Rapp, L. Zhu, A.A. Gewirth, Identifying lithium-air battery discharge products through ^{6}Li solid-state MAS and ^{1}H-^{13}C solution NMR spectroscopy, J. Power Sources 235 (2013) 87–94.

[10] T. Kim, K. Ideta, D. Jung, K. Saito, J.-I. Park, C.K. Rhee, J. Miyawaki, I. Mochida, S.-H. Yoon, Quantitative analysis of BF_4^- ions infiltrated into micropores of activated carbon fibers using nuclear magnetic resonance, RSC Advances 4 (2014) 16726–16730.

[11] Y. Nishiyama, M. Malon, Z. Gan, Y. Endo, T. Nemoto, Proton-nitrogen-14 overtone two-dimensional correlation NMR spectroscopy of solid-sample at very fast magic angle sample spinning, J. Magn. Reson. 230 (2013) 160–164.

[12] T. Matsunaga, I. Matsuda, T. Yamazaki, Y. Ishii, Decoherence optimized tilted-angle cross polarization: A novel concept for sensitivity-enhanced solid-state NMR using ultra-fast magic angle spinning, J. Magn. Reson. 322 (2021) 106857.

[13] R.D. Engardt, G.H. Paine, The effect of eddy currents on NMR line shapes in the presence of self-diffusion, J. Appl. Phys. 51 (1980) 607–609.

[14] W.M. Spees, N. Buhl, P. Sun, J.J.H. Ackerman, J.J. Neil, J.R. Garbow, Quantification and compensation of eddy-current-induced magnetic-field gradients, J. Magn. Reson. 212 (2011) 116–123.

[15] G. Aubert, J.-F. Jacquinot, D. Sakellariou, Eddy current effects in plain and hollow cylinders spinning inside homogeneous magnetic fields: Application to magnetic resonance, J. Chem. Phys. 137 (2012) 154201.

[16] P.M. Aguiar, J.-F. Jacquinot, D. Sakellariou, Experimental and numerical examination of eddy (Foucault) currents in rotating micro-coils: Generation of heat and its impact on sample temperature, J. Magn. Reson. 200 (2009) 6–14.

[17] A. Bielecki, D.P. Burum, Temperature dependence of ^{207}Pb MAS spectra of solid lead nitrate. An accurate, sensitive thermometer for variable-temperature MAS, J. Magn. Reson. A 116 (1995) 215–220.

[18] T. Mildner, H. Ernst, D. Freude, ^{207}Pb NMR detection of spinning-induced temperature gradients in MAS rotors, Solid State Nucl. Magn. Reson. 5 (1995) 269–271.

[19] L.C.M. van Gorkom, J.M. Hook, M.B. Logan, J.V. Hanna, R.E. Wasylishen, Solid-state lead-207 NMR of lead(II) nitrate: Localized heating effects at high magic angle spinning speeds, Magn. Reson. Chem. 33 (1995) 791–795.

[20] B. Langer, I. Schnell, H.W. Spiess, A.-R. Grimmer, Temperature calibration under ultrafast MAS conditions, J. Magn. Reson. 138 (1999) 182–186.

[21] T. Takahashi, H. Kawashima, H. Sugisawa, T. Baba, ^{207}Pb chemical shift thermometer at high temperature for magic angle spinning experiments, Solid State Nucl. Magn. Reson. 15 (1999) 119–123.

[22] P.A. Beckmann, C. Dybowski, A thermometer for nonspinning solid-state NMR spectroscopy, J. Magn. Reson. 146 (2000) 379–380.

[23] N. Iwashita, C.R. Park, H. Fujimoto, M. Shiraishi, M. Inagaki, Specification for a standard procedure of X-ray diffraction measurements on carbon materials, Carbon 42 (2004) 701–714.

[24] S. Brunauer, P.H. Emmett, W. Teller, Adsorption of gases in multimolecular layers, J. Am. Chem. Soc. 60 (1938) 309–319.

[25] K. Kaneko, C. Ishii, M. Ruike, H. Kuwabara, Origin of superhigh surface area and microcrystalline graphitic structures of activated carbons, Carbon 30 (1992) 1075–1088.

[26] K. Ideta, D.-W. Kim, T. Kim, K. Nakabayashi, J. Miyawaki, J.-I. Park, S.-H. Yoon, ^{19}F *ex situ* solid-state NMR study on structural differences in pores of activated carbon series derived from chemical and physical activation processes for EDLCs, J. Phys. Chem. C 124 (2020) 12457–12465.

[27] H. Valdés, M. Sánchez-Polo, J. Rivera-Utrilla, C.A. Zaror, Effect of ozone treatment on surface properties of activated carbon, Langmuir 18 (2002) 2111–2116.

[28] H. Valdés, C.A. Zaror, Ozonation of benzothiazole saturated-activated carbons: Influence of carbon chemical surface properties, J. Hazard. Mater. B137 (2006) 1042–1048.

[29] P. Krawczyk, Effect of ozone treatment on properties of expanded graphite, Chem. Eng. J. 172 (2011) 1096–1102.

[30] T. Kim, C. Ham, C.K. Rhee, S.-H. Yoon, M. Tsuji, I. Mochida, Effects of oxidation and heat treatment of acetylene blacks on their electrochemical double layer capacitances, Carbon 47 (2009) 226–233.

[31] R. Neffati, J.M.C. Brokken-Zijp, Structure and porosity of conductive carbon blacks, Mater. Chem. Phys. 260 (2021) 124177.

[32] J. Rivera-Utrilla, M. Sánchez-Polo, The role of dispersive and electrostatic interactions in the aqueous phase adsorption of naphthalenesulphonic acids on ozone-treated activated carbons, Carbon 40 (2002) 2685–2691.